




ALMA (finally!) discloses a rotating disk+bipolar wind system at the centre of the wind-prominent pPN OH 231.8+4.2

C. Sánchez Contreras¹, J. Alcolea², R. Rodríguez-Cardoso^{1,2},
V. Bujarrabal³, A. Castro-Carrizo⁴, L. Velilla-Prieto⁵,
G. Quintana-Lacaci⁵, M. Santander-García², M. Agúndez⁵ and
J. Cernicharo⁵

¹Centro de Astrobiología (CSIC-INTA), Camino Bajo del Castillo s/n, E-28691 Villanueva de la Cañada, Madrid, Spain
email: csanchez@cab.inta-csic.es

²Observatorio Astronómico Nacional (IGN), Alfonso XII No 3, 28014 Madrid, Spain

³Observatorio Astronómico Nacional (IGN), Ap 112, 28803 Alcalá de Henares, Madrid, Spain

⁴Institut de Radioastronomie Millimetrique, 300 rue de la Piscine, 38406 Saint Martin d'Herès, France

⁵Instituto de Física Fundamental (CSIC), C/ Serrano, 123, E-28006, Madrid, Spain

Abstract. We present interferometric continuum and molecular line emission maps obtained with the Atacama Large Millimeter/submillimeter Array (ALMA) of OH231.8+4.2, a well studied bipolar nebula around an asymptotic giant branch (AGB) star that is key to understand the remarkable changes in nebular morphology and kinematics during the short transition from the AGB to the Planetary Nebula (PN) phase. The excellent angular resolution of our maps (~ 20 mas ~ 30 AU) allows us to scrutinize the central nebular regions of OH231.8+4.2, which hold the clues to understanding how this iconic object assembled its complex nebular architecture. We report, for the first time in this object and others of its kind (i.e. pre-PNe with massive bipolar outflows), the discovery of a rotating circumbinary disk of radius ~ 30 AU traced by NaCl, KCl, and H₂O emission lines. The disk lies at the base of a young bipolar wind with signs of rotation as well. A compact spatially resolved dust disk is found perpendicular to the bipolar outflow. We also identify a point-like continuum source, which likely represents the central Mira star enshrouded by a $\sim 3 R_*$ shell or disk of hot (~ 1400 K) freshly formed dust. The point source is slightly off-centre from the disk centroid, enabling us for the first time to place constraints to the orbital separation of the central binary system.

Keywords. AGB and post-AGB stars, planetary nebulae, mass-loss, rotating disks, binaries, OH 231.8+4.2

1. Introduction

Currently, the PN/pre-PN (pPN) community is reaching full consensus that binaries are needed to help in the production of collimated fast winds (jets) that are in turn primary agents for the breaking of the spherical symmetry during the AGB to PN transition. Rotating structures are expected to form associated with the presence of stellar or substellar companions to mass-losing stars, however, direct empirical confirmation and characterization of such structures is very difficult. To date, rotating circumbinary disks have been found in a population of binary post-AGB stars with near-infrared (NIR)

excess, referred to as disk-prominent post-AGB stars, that curiously lack of massive fast outflows (see e.g. Van Winckel 2017; Bujarrabal *et al.* 2013 and references there in). In this contribution, we report on the first confirmed detection of a rotating disk in a pPN with massive bipolar outflows (referred to as wind-prominent pPN).

OH231.8+4.2 is a well known bipolar nebula around a mass-losing AGB star, QX Pup. QX Pup is a Mira-type variable that as prematurely developed a massive ($\sim 1 M_{\odot}$) pPN-like nebula with a spectacular bipolar morphology and very fast outflows, with velocities of up to a few hundred km s^{-1} that are reached at the tips of large-scale ($\approx 0.1\text{--}0.2$ pc-sized) bipolar lobes. QX Pup is part of a binary system with (at least) one companion, an A0V star (Sánchez Contreras *et al.* 2004), whose presence is probably at the root of the seemingly premature evolution of this object to the next pPN stage, in which the spherical symmetry is broken and high-speed collimated outflows develop. OH231.8+4.2 is located at a distance of $d \sim 1500$ pc.

The structure and kinematics of the molecular envelope of OH231.8+4.2 has been recently characterized with unprecedented detail based on $\sim 0''.2\text{--}0''.3$ -angular resolution continuum and molecular line maps obtained with ALMA (Sánchez Contreras *et al.* 2018). From these observations, we found that the molecular outflow has a structure much more complex than previously thought: we discovered an extravagant array of nested (but not always co-axial) small-to-large scale structures previously unknown that suggest a complex formation history. In the central regions of the nebula, we discovered two main structures: *i*) a compact parcel of gas and dust that surrounds the mass-losing AGB star, referred to as clump *S*, that is selectively traced by certain species, including NaCl; and *ii*) a compact bipolar outflow that emanates from clump *S*, which is selectively traced by SiO. Unlike the large-scale CO outflow, the SiO-outflow is symmetric with respect to the equator and *slow* ($V_{\text{exp}} \lesssim 20 \text{ km s}^{-1}$). The SiO-outflow is younger than the large-scale nebula, which is about ~ 800 yr old.

2. Observations

With the goal of dissecting the central regions of OH231.8+4.2, we observed this object again with the ALMA 12m interferometric array in its most extended configuration during cycle 5 (2017.1.00706.S). Two frequency settings within band 6 ($\sim 242\text{--}261$ GHz and $\sim 217\text{--}234$ GHz, respectively) were used to map molecular line and continuum emission. The data were obtained with 50-52 antennas with baselines ranging from 41.4 m to 16.2 km, resulting in a highest angular resolution of about $\sim 0''.02$. The maximum recoverable scale (MRS) is $\sim 0''.3\text{--}0''.4$.

In the following section, we present the maps of the continuum emission at 261 GHz and of NaCl and SiS/SiO transitions that selectively trace the central regions (down to ~ 30 AU from the central star) of the molecular outflow. Full details on the observations, data reduction and image restoration procedures as well as our in-depth analysis of these and other molecules included in our ALMA dataset are presented in Sánchez Contreras *et al.* (in preparation).

3. Results: a compact rotating disk+outflow system in OH231.8+4.2

3.1. Continuum maps

As known from several previous works, the continuum emission in OH231.8+4.2 is due to dust thermal emission (e.g. SC+18 and references therein). The compact region around QX Pup identified in our previous ALMA maps, clump *S*, is now spatially resolved in two main components: an extended disk-like component, elongated in the direction perpendicular to the bipolar nebula, and an unresolved component (Fig. 1). The dimensions of the extended component are consistent with a circular disk, of radius of ~ 40 AU, inclined

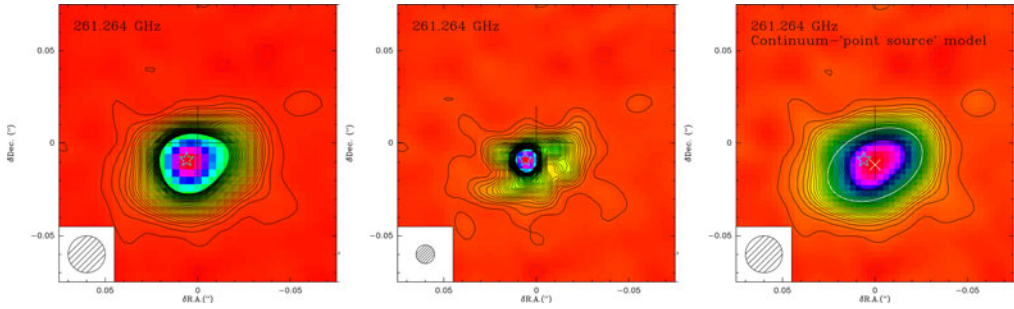


Figure 1. ALMA continuum emission maps at 261.264 GHz. In the left and middle panels, the continuum maps with 20 and 10 mas resolution are shown; level steps are 0.15 mJy/beam $\sim 2.7\sigma$. In the right panel, we show the continuum map with 20 mas resolution after fitting and subtracting a point source model that is located at the position marked by the star-like symbol. The white ellipse represents the size and orientation of the extended disk model that best fits the residual continuum emission map after subtraction of the point source model. Note the offset between the position of the point-like continuum source (starlike symbol) and the center of the disk (white small cross). The shaded circular areas at the bottom-left corner of the maps represent the half-power-beam-width (HPBW). The large black cross marks the phase tracking center of the observations.

$\lesssim 40^\circ$ with respect to the line of sight. This value is very similar to the inclination of the lobes with respect to the plane of the sky known from previous works (e.g. [Kastner et al. 1992](#)), indicating that the disk and the lobes are orthogonal.

The point-like continuum emission is consistent with being partially due to the stellar photosphere of QX Pup ($T_{\text{eff}} \sim 2500$ K, $R_* \sim 2.1$ AU) and to hot (~ 1400 K) dust in its vicinity (within a few stellar radii, $R_d \sim 7.5$ AU). We observe a small offset (~ 6.6 mas) between the centroid of the extended disk and the position of the point-like source. Assuming that the disk is circumbinary and adopting reasonable values for the mass of QX Pup ($m_1 \sim 0.7 M_\odot$) and the A0V companion ($m_2 \sim 2 M_\odot$) we derive from this offset an orbital separation of $a \sim 23$ AU for the binary system.

3.2. Molecular line maps

We have observed a large number of molecular transitions from different species as part of this project. Here, we focus on line emission maps of NaCl and SiS/SiO, some of the molecules that selectively trace the central clump *S* and the compact SiO-outflow, respectively (SC+18).

3.2.1. NaCl

We have detected a total of 8 different transitions of NaCl in different $v=0, 1, 2$, and, tentatively 3, vibrational levels. The lines are weak but they all consistently show a very similar brightness distribution. Taking advantage of this, the lines have been combined to obtain a NaCl line-stacked emission cube with an increased signal-to-noise ratio. As shown in Fig. 2, the NaCl emission arises from a compact region surrounding the extended dust-continuum disk (indicated by the dashed ellipse) consistent with NaCl arising from the surface layers of the dust disk. These layers of the disk are in rotation as indicated by the clear velocity gradient along the equator noticeable in the first-moment map (right panel of Fig. 2); note that the emission from the east side is red-shifted while the west side is blue-shifted. The sense of the rotation of the circumbinary NaCl-disk, with its east (west) side receding from (approaching to) us, is the same as that of the SiO-maser rotating torus found in the pulsating layers of QX Pup ([Sánchez Contreras et al. 2002](#)).

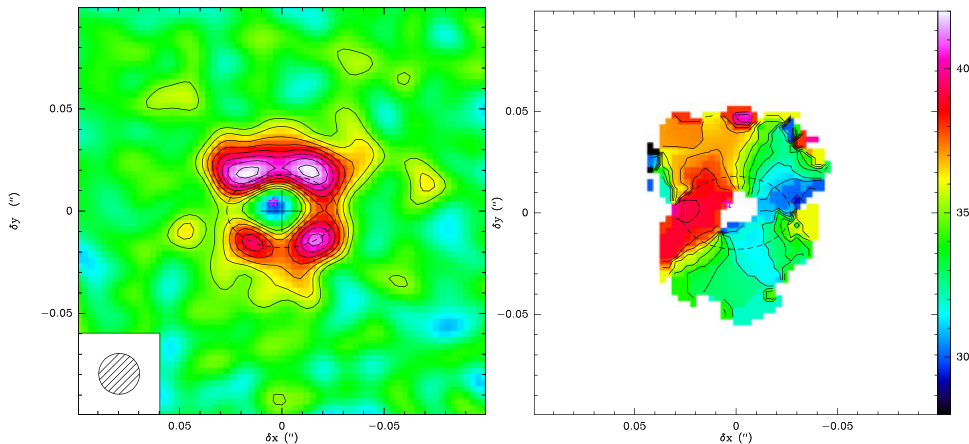


Figure 2. ALMA data of NaCl after stacking together the individual NaCl transitions detected in this work. Left) order-zero moment map over the $V_{\text{LSR}}=[24:46]$ km s $^{-1}$ velocity range; contours are 2σ , 3σ ,... by 1σ ($\sigma=1.7$ mJy/beam km s $^{-1}$). Right) first-moment map; contours go from $V_{\text{LSR}}=28$ to 43 by 1 km s $^{-1}$. The wedge indicates the colour- V_{LSR} scale. Maps are rotated by 25° clockwise so the symmetry axis of the nebula is vertical. The center of the dust disk (dashed ellipse) inferred from the continuum emission maps is marked with a cross (R.A.=07^h42^m16^s91500 and Dec.=−14°42′50″.0716, J20000) and has been adopted as the origin of positional offsets here and in Fig. 3.

The rotation velocity deduced from the NaCl maps is about $V_{\text{rot}}\sim 4$ km s $^{-1}$ at a mean radial distance of ~ 40 AU. In addition to rotation, there are also expansive motions in the circumbinary NaCl-disk with a strikingly low expansion speed of $V_{\text{exp}}\sim 3$ km s $^{-1}$.

To better constrain the geometry, kinematics, and physical conditions of the rotating disk layers probed by NaCl, we have compared the ALMA NaCl maps with the predictions of a LTE radiative transfer model for this species. We have approximated the geometry of the NaCl-emitting volume as two co-axial tori of radius ~ 30 –35 AU displaced along the nebula axis from the continuum disk midplane by ~ 20 AU, emulating the two surface layers (above and below) the disk where the NaCl is detected. The overall kinematics is reasonably well described with a composite velocity field that includes rotation and expansion in the equatorial plane. For a uniform temperature of $T_{\text{rot}}\sim 400$ –500 K, deduced from an independent analysis of the different NaCl transitions detected, and adopting a fractional NaCl-to-H $_2$ abundance of $X(\text{NaCl})\sim 5\times 10^{-9}$ (SC+18), we derive average H $_2$ densities of $\approx 10^9$ cm $^{-3}$, resulting in a total mass of the disk’s surface layers of about $2\times 10^{-3} M_{\odot}$. The angular resolution of our ALMA data is still insufficient to study the radial variations of the model parameters across the disk layers, in particular, we cannot infer whether the rotation follows a Keplerian or a sub-Keplerian velocity law. The presence of expansion suggests sub-Keplerian rotation (e.g. Kervella *et al.* 2016), which would then imply a lower limit to the central dynamic mass of $\sim 0.7 M_{\odot}$.

In addition to NaCl, we have found two other molecular species that selectively trace the rotating equatorial structure at the core of OH231.8+4.2, namely, potassium chloride (KCl, i.e. another salt) and water (H $_2$ O); these species are potentially unique tools for identifying disks and measuring their kinematics in pPNe.

3.2.2. $\text{SiS } v=0$ and $\text{SiO } v=1$

The compact ($\sim 1''\times 4''$) bipolar outflow discovered in SC+18 is traced by several rotational transitions in the $v=0$ and $v=1$ vibrational states of SiO and SiS (including

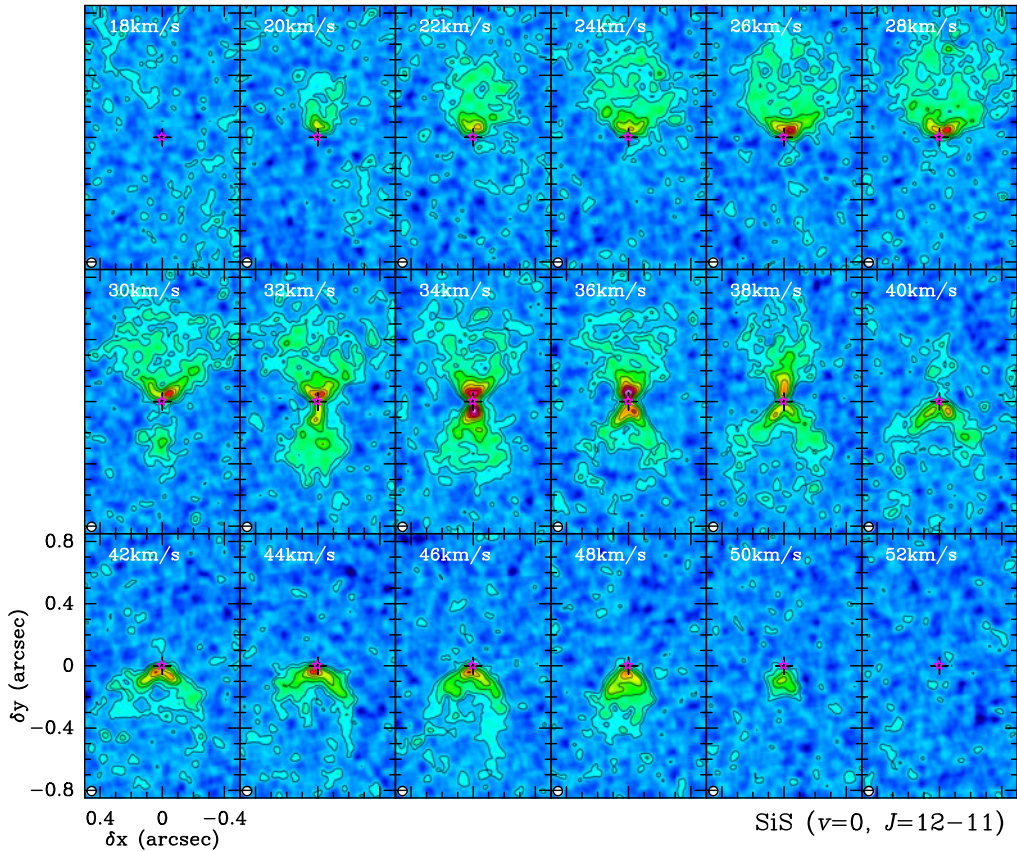


Figure 3. SiS $v=0$ ($J=12-11$) velocity-channel maps (contours: 2σ , 4σ ,... by 4σ ; $\sigma=0.57$ mJy/beam). Natural weighting and tapering (with a tapering distance of 5700 m) have been used to restore the emission maps with a half-power clean beam width of $\text{HPBW}=0''.06 \times 0''.06$.

some isotopologues). We refer to this component as the SiO/SiS-outflow (hereafter, SS-outflow). In this contribution, we discuss the SiS $v=0$, $J=12-11$ line, which best delineates the dense walls of the bipolar SS-outflow, and the vibrationally excited SiO $v=1$, $J=6-5$ line, which traces the innermost layers of the SS-outflow (i.e. closer to the center) where the gas is presumably denser and hotter.

The SiS $v=0$, $J=12-11$ maps (Fig. 3) show that the lobes have a conical geometry at their base, consistent with a wide opening angle ($\theta \sim 90^\circ$) wind, and a more rounded morphology at their tips. The SS-outflow emerges from the surface layers of the rotating equatorial disk, where the SiS $v=0$, $J=12-11$ and NaCl emission partially overlap. We find low-to-moderate expansion velocities throughout the SS-outflow. From a simple a spatio-kinematic model of the SS-outflow to fit the SiS $v=0$, $J=12-11$ data we deduce a gradual outward acceleration of the gas along the lobes up to a terminal expansion speed of about $\sim 17 \text{ km s}^{-1}$, which is reached at a radial distance of ~ 250 AU. The radial expansion continues at constant velocity beyond this point. We have constrained the inclination of the SS-outflow to values around $\sim 30^\circ-35^\circ$ and its kinematical age to about one hundred years at the base (to be compared with the 800 yr age of the large-scale CO outflow).

Our maps from the vibrationally excited SiO $v=1$, $J=6-5$ line show emission arising from a compact elongated region of dimensions $\sim 0''.05 \times 0''.12$ oriented along $PA \sim 25^\circ$, consistent with a bipolar wind running inside the hollow rotating disk traced by the salts and water. The kinematics at the base of the SS-outflow as traced by SiO $v=1$, $J=6-5$ emission is predominantly expansive but the signature of rotation is also present, particularly in regions close to the equator. This was somehow expected given the SiO and NaCl emission overlap at the base of the SS-outflow.

4. Discussion

NaCl beyond the dust formation zone. It is well known that in normal AGB stars, NaCl forms by equilibrium chemistry near the stellar photosphere and that this species disappears from the gas phase rapidly as it gets incorporated into dust grains given its refractory character. In OH231.8+4.2, we observe NaCl on the surface of the dust disk, which is beyond the region of massive dust formation where NaCl should be significantly gas depleted as a consequence of condensation onto the grains. At the base of the SS-outflow, NaCl is co-spatial with SiO (and SiS), which is a well known shock tracer, suggesting that shocks are probably efficiently extracting NaCl from grains and returning it to the gas phase.

Low expansion velocity in the disk. Another surprising result from this work is the extremely low expansion velocity ($V_{\text{exp}} \sim 3 \text{ km s}^{-1}$) measured at the surface layers of the rotating disk, at relatively large radial distances from the center of $\sim 40 \text{ AU} \sim 6 \times 10^{14} \text{ cm} \sim 20 R_*$. At these distant regions, clearly beyond the massive dust condensation (wind acceleration) zone, the wind velocity of a normal O-rich AGB star (like, e.g., IK Tau, [Decin et al. 2010](#)) should be close to the terminal velocity, that is, close to $\sim 15\text{--}25 \text{ km s}^{-1}$ for a high-mass loss rate object like OH231.8+4.2. The reason for such inefficient wind acceleration in OH231.8+4.2 is unknown (it may be caused by the presence of very optically thick dust or very large grains along the equator), but, as it is shown in the next paragraph, a low wind velocity turns out to be essential to promote the formation of an equatorially dense circumbinary structure as a result from wind Roche Lobe Overflow (wRLOF) mass transfer ([Mohamed & Podsiadlowski 2007](#)) in the central binary system.

Formation of an equatorial density enhanced (EDE) region. In addition to an extremely low wind velocity, OH231.8+4.2 brings together other favorable conditions for the formation of a dense equatorial structure as a result of wRLOF mass transfer, namely: a very massive companion ($q=m_1/m_2 \sim 0.4 < 1$) and comparable sizes of the dust condensation radius ($R_d \sim 7.5 \text{ AU}$) and the Roche lobe radius ($r_L \sim 7 \text{ AU}$, for $a \sim 23 \text{ AU}$; [Eggleton 1983](#)). As shown e.g. in the recent work by [El Mellah et al. \(2020\)](#), these are key parameters for effective mass transfer from QX Pup to the companion and the eventual compression of the AGB wind on the orbital plane to form an EDE.

The SS-outflow. Given its properties (low-velocity and wide opening angle), the SS-outflow could simply result from the confinement of the on-going AGB wind by the dense equatorial torus (as in the so-called Generalized Interacting Stellar Winds scenario of PN-shaping, see e.g. [Balick and Frank 2002](#)). The absence of fast jet-like ejections (together with the lack of classical accretion indicators, such as H α emission from the nucleus) rules out high-rate accretion by a compact object *at present*. The situation was clearly different ~ 800 yr ago, when the large-scale bipolar nebula was shaped and accelerated up to velocities of $\approx 400 \text{ km s}^{-1}$, a process that necessarily required accretion on (and jet-launching from) a main-sequence companion. Perhaps the accretion disk around the companion has been exhausted in recent times. Alternatively, as we proposed in [Sánchez Contreras et al. \(2004\)](#), OH231.8+4.2 could be at present in a low-rate accretion

(or ‘quiescent’) state in which the disk around the companion is steadily building up its mass but there is no effective disk-to-companion accretion (and no jet launching), a situation that occurs in other astrophysical systems known to go through alternating accretion outburst and post-outburst (quiescent) states (like FU Ori objects and symbiotics stars, e.g. Hartmann & Kenyon 1996).

Acknowledgements

This work is part of the I+D+i projects PID2019-105203GB-C22 and PID2019-105203GB-C21, funded by the Spanish MCIN/ AEI/10.13039/501100011033.

References

- Alcolea, J., Bujarrabal, V., Sánchez Contreras, C., Neri, R., and Zweigle, J. 2001, *A&A*, 373, 932
- Balick, B., and Frank, A. 2002, *ARA&A*, 40, 439
- Bujarrabal, V., Alcolea, J., Van Winckel, H., et al. 2013, *A&A*, 557, A104
- Decin, L., Justtanont, K., De Beck, E., et al. 2010, *A&A*, 521, L4
- Eggleton, P. P. 1983, *ApJ*, 268, 368
- El Mellah, I., Bolte, J., Decin, L., et al. 2020, *A&A*, 637, A91.
- Hartmann, L. & Kenyon, S. J. 1996, *ARA&A*, 34, 207
- Kastner, J. H., Weintraub, D. A., Zuckerman, B., et al. 1992, *ApJ*, 398, 552
- Kervella, P., Homan, W., Richards, A. M. S., et al. 2016, *A&A*, 596, A92
- Mohamed, S. & Podsiadlowski, P. 2007, 15th European Workshop on White Dwarfs, 372, 397
- Sánchez Contreras, C., Desmurs, J. F., Bujarrabal, V., et al. 2002, *A&A*, 385, L1
- Sánchez Contreras, C., Gil de Paz, A., and Sahai, R. 2004, *ApJ*, 616, 519
- Sánchez Contreras, C., Alcolea, J., Bujarrabal, V., et al. 2018, *A&A*, 618, A164
- van Winckel, H. 2017, Planetary Nebulae: Multi-Wavelength Probes of Stellar and Galactic Evolution, Proceedings of the International Astronomical Union, IAU Symposium, 323, 231